Optimization of the Johnson–Mehl–Avarami Equation Parameters for α-Ferrite to γ-Austenite Transformation in Steel Welds Using a Genetic Algorithm

A. KUMAR, S. MISHRA, J.W. ELMER, and T. DEBROY

A nonisothermal Johnson–Mehl–Avarami (JMA) equation with optimized JMA parameters is proposed to represent the kinetics of transformation of α-ferrite to γ-austenite during heating of 1005 steel. The procedure used to estimate the JMA parameters involved a combination of numerical heat-transfer and fluid-flow calculations, the JMA equation for nucleation and growth for nonisothermal systems, and a genetic algorithm (GA) based optimization tool that used a limited volume of experimental kinetic data. The experimental data used in the calculations consisted of phase fraction of γ-austenite measured at several different monitoring locations in the heat-affected zone (HAZ) of a gas tungsten arc (GTA) weld in 1005 steel. These data were obtained by an *in-situ* spatially resolved X-ray diffraction (SRXRD) technique using synchrotron radiation during welding. The thermal cycles necessary for the calculations were determined for each monitoring location from a well-tested three-dimensional heat-transfer and fluid-flow model. A parent centric recombination (PCX) based generalized generation gap (G3) GA was used to obtain the optimized values of the JMA parameters, *i.e.*, the activation energy, pre-exponential factor, and exponent in the nonisothermal JMA equation. The GA based determination of all three JMA equation parameters resulted in better agreement between the calculated and the experimentally determined austenite phase fractions than was previously achieved.

I. INTRODUCTION

PROPERTIES of carbon-manganese steels are affected by the phase fractions of α-ferrite and γ-austenite. These phase fractions change due to heating and cooling during the processing of steels. The nonisothermal Johnson–Mehl–Avrami (JMA) equation has been used often to represent phase transformation behavior in many systems involving nucleation and growth such as the α-ferrite to γ-austenite transformation in C-Mn steels during heating.[1] However, the JMA equation contains three unknown parameters, *i.e.*, the activation energy, pre-exponential factor, and JMA exponent. At present, there is no unified method to assign the values of these important parameters. While the nonisothermal JMA equation can serve as a basis for quantitative calculations in many important systems, without reliable values of these three constants, the utility of the equation is considerably diminished.

Elmer *et al.*[1] calculated the values of the pre-exponential factor and exponent of the nonisothermal JMA equation for the α-ferrite to γ-austenite transformation in C-Mn steels. Their approach assumed a value of the activation energy suggested by Nath *et al*,[2] who showed that the apparent activation energy for the α-ferrite to γ-austenite transformation will be different from that for the diffusion of carbon in austenite due to the combined effects of nucleation and growth. Since Elmer *et al.*[1] calculated the values of the other two JMA parameters, a fairly straightforward graphical technique could be used. However, since the transformation rate is very sensitive to the values of all three JMA parameters, none of these parameters can be assumed to be known.

The goal of the present work is to estimate all three parameters of the JMA equation, *i.e.*, the activation energy of transformation, the pre-exponential factor, and the exponent in the nonisothermal JMA equation through an inverse modeling approach. The approach involves a combination of a genetic algorithm (GA) based optimization model, a temperature field calculation model, a phase fraction calculation model, and experimentally measured kinetic data. The experimental data used in the calculations consisted of phase fraction of γ-austenite measured at several different monitoring locations in the heat-affected zone (HAZ) of a gas tungsten arc (GTA) weld in 1005 steel. These data were obtained by an *in-situ* spatially resolved X-ray diffraction (SRXRD) technique using synchrotron radiation during the welding.

De and DebRoy,[3] Kumar *et al.*,[4] and Kumar and DebRoy[5] recently developed inverse models to calculate various unknown input parameters such as the arc efficiency, effective thermal conductivity, and effective viscosity for numerical thermofluid modeling of the welding processes using derivative based optimization techniques. A drawback of these techniques is their occasional convergence to a local solution.[6] Furthermore, an appropriate initial guess of the unknown variables is needed to achieve the global optimal solution. The ability of the GA to find the global optimal solution independent of the initial guessed values[6,7] makes GA unique for estimating the JMA parameters.

In order to obtain the values of all three JMA parameters, three interactive computational modules are embedded in the present scheme: first, for the analysis of heat transfer and fluid flow;[8–21] second, for the calculation of phase transformation using the JMA equation;[1,8,21] and third, for obtaining the optimized values of these parameters. A multivariable optimization scheme is used, which is based on the parent centric recombination (PCX) based generalized generation gap (G3)

A. KUMAR and S. MISHRA, Graduate Students, and T. DEBROY, Professor, Department of Materials Science and Engineering are with The Pennsylvania State University, University Park, PA 16802. Contact e-mail: debroy@psu.edu J.W. ELMER, Group Leader, Materials Joining, is with the Lawrence Livermore National Laboratory, Livermore, CA 94551.

Manuscript submitted June 3, 2004.

GA model.[22,23] The approach adopted here is inherently different from the neural network technique where the input and output variables are related through a set of hidden nodes and their relationships do not necessarily have to comply with any physical law. In contrast, when the optimization algorithm embodies a phenomenological model of heat transfer and fluid flow and the nonisothermal JMA equation to represent the transformation of α-ferrite to γ-austenite, the output weld pool geometry and microstructure are related by well-established laws. Thus, determination of the JMA parameters will be based on well-established scientific principles.

II. MATHEMATICAL MODEL

The calculation of all three JMA parameters through a systematic search algorithm from a limited volume of experimental data requires calculations of the thermal cycles and austenite phase fractions during heating. The details of the heat-transfer and fluid-flow calculation procedure and the nonisothermal phase transformation calculations are widely available in the literature,[1,8–21] so only a brief summary of the salient features of the calculations specific to the JMA parameter search is included here.

A. *Calculation of Temperature Field and Thermal Cycles*

The temperature field and thermal cycles are calculated using an extensively tested three-dimensional (3-D) numerical heat-transfer and fluid-flow model.[8–21] In this model, the transient nature of the problem is transformed to steady-state mode by using a coordinate system moving with the heat source.[20] The governing equations of conservation of mass, momentum, and energy in three dimensions are discretized using the power-law scheme.[24] The computational domain is divided into small rectangular control volumes. Discretized equations for the variables are formulated by integrating the corresponding governing equation over the control volumes. The detailed method of discretizing the governing equations is available in the literature.[20] The discretized equations are solved using the SIMPLE algorithm[24] to obtain temperature and velocity fields.

B. *Calculation of Austenite (γ) Phase Fraction*

For α-ferrite to γ-austenite transformation during heating of low-carbon steels, the transformation path involves $\alpha \rightarrow (\alpha + \gamma) \rightarrow \gamma$. The transformation to austenite starts at 993 K and finishes at 1155 K in 1005 steel. In the $\alpha + \gamma$ two-phase region, the equilibrium austenite fraction, F, is lower than 1 and can be calculated from the corresponding phase diagram.[1] For 1005 steel, the equilibrium austenite fraction, $F(T)$, at any particular temperature, is given by

$$F(T) = \frac{0.05 - C_\alpha(T)}{C_\gamma(T) - C_\alpha(T)} \qquad [1]$$

where $C_\alpha(T)$ and $C_\gamma(T)$ represent the equilibrium carbon concentrations of α and γ phases, respectively, at any particular temperature, T (K). The values of $C_\alpha(T)$ and $C_\gamma(T)$ are obtained from the phase diagram as follows:

$$C_\alpha(T) = -1.198 \times 10^{-4} T + 0.142 \qquad [2]$$

$$C_\gamma(T) = 1.501 \times 10^{-5} T^2 - 3.666 \times 10^{-2} T + 22.356 \qquad [3]$$

The austenite phase fraction, fr, at selected locations in the weld HAZ is calculated using the nonisothermal JMA equation:[1]

$$\frac{fr(t_i)}{F_i} = 1 - \exp\left\{-\left[k_0 \times \exp\left(-\frac{Q}{RT_i}\right) \times (\Delta t + \tau_i)\right]\right\} \quad \text{for } 1 \le i \le m \qquad [4]$$

where T_i is the temperature for the ith interval (K), F_i is the equilibrium fraction of austenite at temperature T_i, k_0 is a pre-exponential constant (s^{-1}), Q is the activation energy for phase transformation (kJ/mol), R is the gas constant, Δt is the time interval (s), m is the number of time-steps in the thermal cycle, and n is the JMA exponent. The time constant, τ_i, is given by

$$\tau_i = \frac{\sqrt[n]{-\ln\left[1 - \frac{fr(t_{i-1})}{F_i}\right]}}{k_0 \times \exp\left(-\frac{Q}{RT_i}\right)} \qquad [5]$$

where $fr(t_{i-1})$ is the austenite phase fraction calculated at the end of the $(i-1)$th time-step. Equation [4] represents the austenite phase fraction for the time t_i at a given location, and requires the thermal cycle at this location to be known.

C. *GA as an Optimization Model*

The GA based optimization of the three JMA parameters involves a systematic global search for these parameters aimed at minimizing the following objective function, $O(f)$:

$$O(f) = \sum_{k=1}^{p} \sum_{l=1}^{q} \left[fr^e(x_k, y_l, 0) - fr^c(x_k, y_l, 0)\right]^2 \qquad [6]$$

where $fr^c(x_k, y_l, 0)$ and $fr^e(x_k, y_l, 0)$ represent the calculated and experimental values of austenite phase fractions at locations $(x_k, y_l, 0)$, respectively. In the Cartesian coordinate system used in the present study, $(x_k, y_l, 0)$ represents the top surface of the specimen. In Eq. [6], the value of p is 2 as the experimental austenite phase fraction values given in Table I are for two x locations of -5.0 and 0.0 mm, and the value of q is 5 as five different y locations are considered for each x location. The objective function, $O(f)$, in Eq. [6] is a function of the three JMA parameters, *i.e.*, activation energy for phase transformation, Q; the JMA equation exponent, n; and the pre-exponential constant, k_0.

$$\{f\} = (f_1, f_2, f_3) = \left(\frac{Q}{Q_r}, \frac{n}{n_r}, \frac{k_0}{k_r}\right) \qquad [7]$$

Table I. Experimental Data for Austenite (γ) Phase Fractions along $x = -5.0$-mm and $x = 0.0$-mm Lines on the Top Surface ($z = 0.0$)

Location (mm)	γ-Phase Fraction	Location (mm)	γ-Phase Fraction
(−5.0, 1.25, 0.0)	0.691	(0.0, 6.25, 0.0)	1.000
(−5.0, 1.75, 0.0)	0.475	(0.0, 6.50, 0.0)	0.821
(−5.0, 2.25, 0.0)	0.284	(0.0, 6.75, 0.0)	0.331
(−5.0, 2.75, 0.0)	0.149	(0.0, 7.00, 0.0)	0.198
(−5.0, 3.25, 0.0)	0.050	(0.0, 7.25, 0.0)	0.070

Table II. Terminology Used in GA

Biological Terms	Equivalent Welding Variables and Representation in GA
Genes: units containing hereditary information	in the form of nondimensional variables, f_1, f_2, and f_3, *e.g.*, $f_1 = Q/Q_r = 1.10$; $f_2 = n/n_r = 1.70$; $f_3 = k_0/k_r = 1.56$
Chromosome/individual: a number of genes folded together	a set of input variable values taken together, *i.e.*, (1.10, 1.70, 1.56)
Population: collection of many chromosomes/ individuals	collection of multiple sets: (1.10, 1.70, 1.56) (1.20, 1.54, 1.65) (1.23, 1.65, 1.75)
Parents: chromosomes/ individuals participating for creating new individuals (or offsprings)	Parents: *e.g.*, (1.10, 1.70, 1.56) (1.23, 1.65, 1.75)
Fitness value: value of fitness function determines if a chromosome/individual survives or dies	objective function or fitness function: calculated for each set of input variables using Eq. [3]

In Eq. [7], the reference values, Q_r, n_r, and k_r, represent the order of magnitude of the JMA parameters. The activation energy for diffusion of carbon in austenite,[2] Q_r (135 kJ/mol), is taken as a reference value of Q. The reference value of the pre-exponential constant, k_r, is taken to be equal to the value reported in the literature[2] (*i.e.*, $\ln(k_r) = 9.26$). The value of n_r is taken as 1.0, since this value is thought to represent the order of magnitude of n. Note that Eq. [7] is made nondimensional so that all three dimensionless JMA parameters have a comparable order of magnitude values. This procedure aids in the global search for the JMA parameters by scaling down the objective functions. It allows starting values of JMA parameters that are very far off from the final optimized values, thus improving the robustness of the calculation scheme.

A G3 model using a PCX operator[22,23] was used in the present study to calculate the optimized values of the three JMA parameters. This model was chosen because it has been shown to have a faster convergence rate on standard test functions as compared to other evolutionary algorithms.[22,23] A detailed description of this model is available in the literature[22,23] and is not included here. Specific application of GA for the determination of the JMA parameters is given in Appendix A.

The various terms used to describe GA are explained in Table II. The calculation starts with an arbitrarily assumed initial population of sets of three JMA parameters. The final aim is to find the solutions of all three JMA parameters through a systematic global search that will give the least error between the calculated and experimentally obtained austenite phase fractions. The flow chart of the calculation scheme is presented in Figure 1. The population converges to a set of optimal solutions through an iterative scheme involving a PCX operator based recombination scheme.

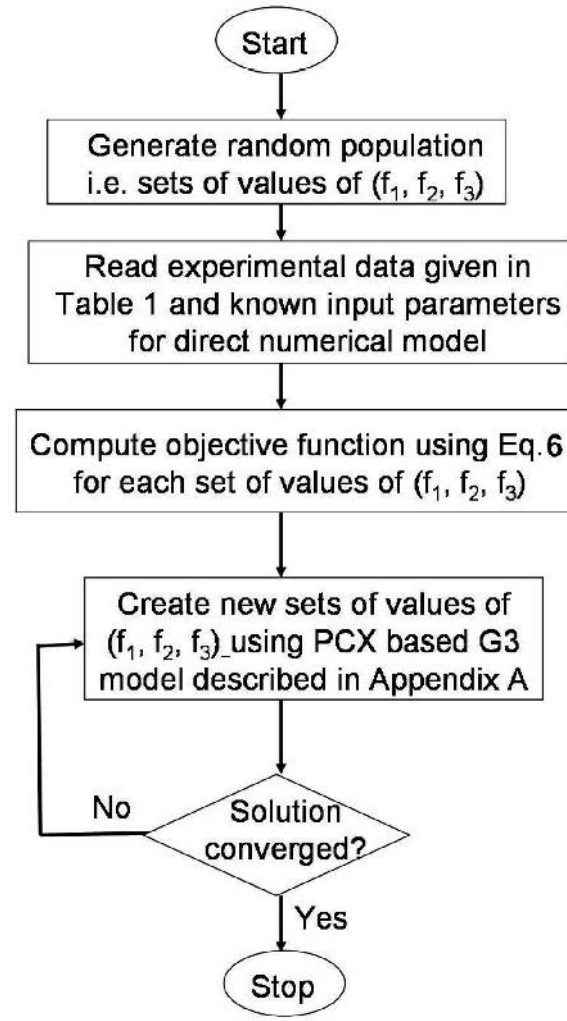

Fig. 1—Flow chart showing the calculation procedure. Note that $(f_1, f_2, f_3) = \left(\frac{Q}{Q_r}, \frac{n}{n_r}, \frac{k_0}{k_r}\right)$.

III. RESULTS AND DISCUSSION

A. *Calculation of Temperature Field and Thermal Cycles*

The GTA welds have been made on cylindrical forged bar samples of AISI 1005 steel. The composition of the steel was 0.05C, 0.31Mn, 0.18Si, 0.11Ni, 0.10Cr, 0.009P, 0.008Cu, 0.005S, <0.005Al, <0.005Nb, <0.005Mo, <0.005Ti, and <0.005V by wt pct. These samples were machined from 10.8-cm-diameter forged bar stock into welding samples, 12.7-cm long and 10.2-cm diameter. Circumferential welds were then made on the cylindrical steel bars in an environmentally sealed chamber to avoid atmospheric contamination of the weld. The welding parameters used are given in Table III. Further details of the welding experiments and the errors involved in the measurements have been discussed elsewhere.[1,25]

In-situ SRXRD experiments provided direct observation of welding induced phase transformations.[1] Figure 2 shows an experimentally measured phase map in the HAZ on the top surface of GTA weld in AISI 1005 C-Mn steel.[1] This map shows one half of the weld HAZ, since the heat flow is considered to be symmetric about the centerline of the weld, and gives quantitative information about the phase transformations that are occurring during both heating and cooling. The weld pool boundary is marked by the solidus isotherm (1779 K), while the A1 (993 K) and A3 (1155 K) isotherms identify the

Table III. Summary of GTA Welding Parameters Used in the SRXRD Experiments

Maximum current (A)	130
Background current (A)	90
Weld voltage (V)	17.5
Welding electrode	W-2 pct Th
Electrode diameter (mm)	4.7
Torch polarity	DC, electrode negative
Pulsing frequency (Hz)	300
Peak on time (pct)	50
Shielding gas	helium
Travel speed (mm/s)	0.6
Resulting fusion zone width (mm)	~9

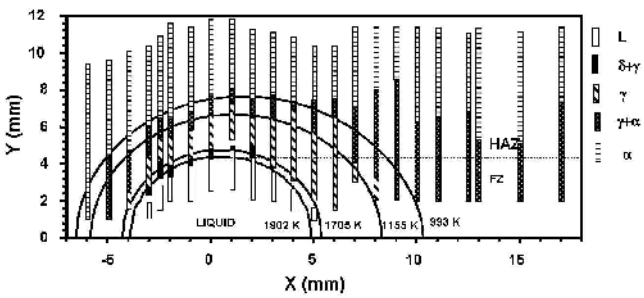

Fig. 2—SRXRD semiquantitative phase map plotting the volume fraction of austenite in the HAZ. The calculated isotherms using the 3-D dimensional heat-transfer and fluid-flow model are superimposed on the map correspond to the liquidus (1802 K), the $\gamma/(\gamma + \delta)$ phase boundary (A4, 1705 K), the $\gamma/(\alpha + \gamma)$ phase boundary (A3, 1155 K), and the eutectoid temperature (A1) (993 K).

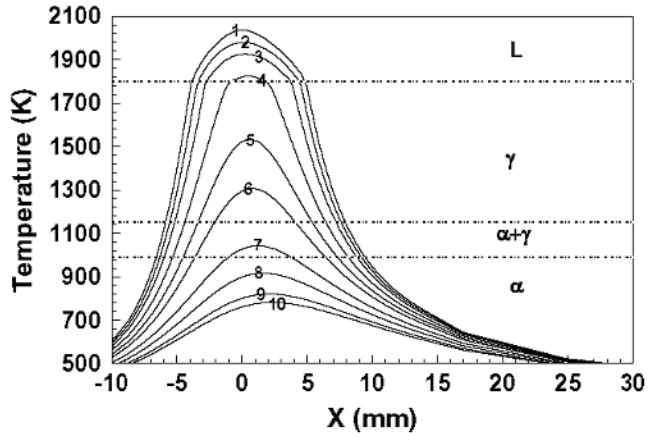

(*a*)

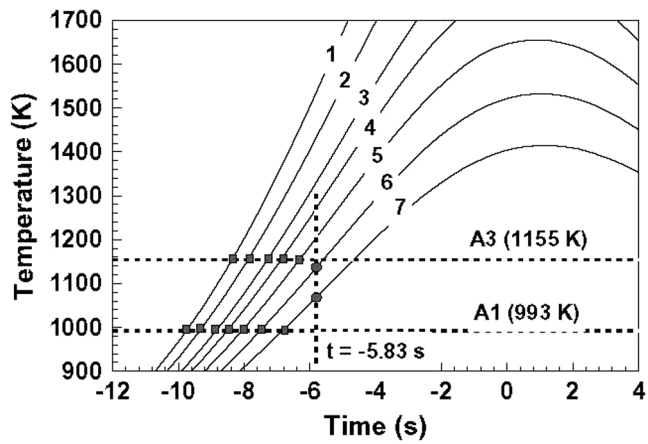

(*b*)

Fig. 3—(*a*) Temperature *vs* distance plot showing temperature cycles parallel to the welding direction at various *y*-axis offset from the weld centerline of (1) 0 mm, (2) 2 mm, (3) 3 mm, (4) 4 mm, (5) 5 mm, (6) 6 mm, (7) 7 mm, (8) 8 mm, (9) 9 mm, and (10) 10 mm. (*b*) Calculated thermal cycles at different *y* locations along $x = -3.5$-mm path. 1: $y = 3.25$ mm; 2: $y = 3.75$ mm; 3: $y = 4.25$ mm; 4: $y = 4.5$ mm; 5: $y = 4.75$ mm; 6: $y = 5.00$ mm; and 7: $y = 5.50$ mm. Time equal to zero was arbitrarily selected to correspond to the heat source location at $x = 0$ in Fig. 3(a).

equilibrium start and finish locations for the ferrite to austenite ($\alpha \rightarrow \gamma$) transformation. The calculated solidus isotherm is found to identify the weld pool boundary. Furthermore, the austenite start and finish boundaries shown in the measured data agreed well with the corresponding equilibrium temperatures, A1 and A3, respectively, after taking kinetic considerations into account. Thus, the temperature field obtained from the 3-D heat-transfer and fluid-flow model is thought to be reliable and was used in the phase transformation calculations.

After obtaining the steady-state temperature field, the thermal cycle at any given location (*x, y, z*) was calculated using the following equation:

$$T(x, y, z, t_2) = \frac{T_s(\xi_2, y, z) - T_s(\xi_1, y, z)}{\xi_2 - \xi_1} V_s(t_2 - t_1) + T(x, y, z, t_1) \quad [8]$$

where $T(x, y, z, t_2)$ and $T(x, y, z, t_1)$ are the temperatures at times t_2 and t_1, respectively; $T_s(\xi_1, y, z)$ and $T_s(\xi_2, y, z)$ are the steady-state temperatures at coordinates (ξ_1, y, z) and (ξ_2, y, z), respectively; V_s is the welding speed; and $(\xi_2 - \xi_1)$ is the length of the weld produced in time $(t_2 - t_1)$.

The calculated thermal cycles at different locations in the HAZ are shown in Figures 3(a) and (b). Figure 3(a) plots the calculated temperatures parallel to the welding direction at the top surface for locations starting at the weld centerline and moving out to a distance of 10 mm from the weld centerline. The peak temperature in the weld pool is 2036 K. The temperature drops to the liquidus (1802 K) at the fusion boundary at $y = 4.4$ mm, and it then continues to decrease to the A1 temperature (993 K) at the $y = 7.7$-mm position. The thermal profiles corresponding to the heating side of the weld, calculated parallel to the welding direction, are further plotted in Figure 3(b) at different HAZ locations from $y = 3.25$ to 5.5 mm. In this plot, the time coordinate, parallel to the welding direction, was calculated from the distance coordinate by dividing the distance along the *x*-axis by the welding speed. Here, the time equal to zero corresponds to the heat source location identified in Figure 3(a) as $x = 0$. The peak temperature and heating rates plotted for various locations in Figures 3(a) and (b) show that both parameters decrease with increasing distance from the weld centerline. These variations in thermal cycles are responsible for the spatial variation of the austenite phase fraction in the HAZ.

In order to illustrate how the temperature profiles influence HAZ phase transformations, the thermal cycles that contribute

Table IV. Different Sets of Unknown JMA Parameters Calculated by the Proposed GA Model by Using Different Initial Range of JMA Parameters

Initial Range of JMA Parameters			Optimal Values of JMA Parameters			Objective
Q (kJ/mol)	n	Ln (k_0)	Q (kJ/mol)	n	Ln (k_0)	Function, $O(f)$
100.00 to 150.00	1.00 to 2.50	11.50 to 14.73	99.64	1.12	11.07	5.84×10^{-2}
50.00 to 550.00	2.50 to 3.50	0.00 to 11.50	100.02	1.14	11.27	5.94×10^{-2}
50.00 to 450.00	1.50 to 3.50	10.00 to 15.00	100.12	1.14	11.30	5.96×10^{-2}

to the $\alpha \rightarrow \gamma$ transformation were calculated for different locations along the SRXRD path perpendicular to the weld at the $x = -3.5$-mm ($t = -5.83$ s) location. Figure 3(b) shows these thermal cycles where each thermal cycle was calculated parallel to the welding direction to represent the heating cycle for the material up to the $x = -3.5$-mm location. The portion of the thermal cycle responsible for the transformation up to these points is indicated by the lines between the solid squares at the transformation start temperature (A1), the solid squares at the transformation finish temperature (A3), and the circles that correspond to the location where the SRXRD data were taken. The difference in paths leads to the variation in the heating rate and thus a variation in the austenite fraction at the different y locations. The calculated thermal profiles, as illustrated in Figure 3(b), represent the type of data that are used in conjunction with the additional SRXRD data to obtain the unknown JMA parameters for the $\alpha \rightarrow \gamma$ transformation in the HAZ of the 1005 steel weld.

B. *Calculation of the JMA Parameters by G3 Algorithm*

The GA approach is a population based search technique where a population consists of many individuals. Here, each individual represents a set of randomly chosen values of the three JMA parameters. In order to generate the initial random population to start the calculations, the values of the three JMA parameters were initialized, guided by their values reported in the literature.[1] The initial ranges for these variables chosen are as follows: k_0 between 1.0×10^5 and 2.5×10^5 s^{-1}, Q between 100.0 and 150.0 kJ/mol, and n between 1.0 and 2.5. All the runs were conducted using several random seeds to achieve a convergence limit, where 20 pct of the individuals of the total population reached an objective function value (fitness) of less than 7.0×10^{-2}. The chosen value of the objective function (fitness) ensured sufficient accuracy within the practical limits of the experimental errors.

Elmer *et al.*[1] used kinetic data taken along seven paths in the weld HAZ ranging from a starting location ahead of the weld at $x = -5.0$ mm to the center of the weld at $x = 0.0$ mm. These data were used to calculate two of the three JMA parameters for the 1005 steel weld. Initially, kinetic data for only two x locations were used in the analysis to check if GA can estimate all three JMA parameters from a limited volume of experimental data. These locations were chosen near the two extremes of the range of x values used by Elmer *et al.*,[1] *i.e.*, at x equal to -5.0 and 0.0 mm in order to include the maximum possible variation in the extent of transformation. It is thought that if the data corresponding to very low and very high transformations are used for the determination of the JMA parameters, the austenite fractions at intermediate transformations could be predicted. Table IV lists the optimal values of JMA parameters computed with several different combinations of the initial values of the JMA parameter sets. Various values of the JMA exponent, n, have been reported in the literature for the α-ferrite to γ-austenite transformation during heating. Christian[26] suggested that the value of n should lie between 1.5 and 2.5 for diffusion-controlled phase transformations. Elmer *et al.*[1] determined n to be 1.43 for α-ferrite to γ-austenite transformation in the 1005 steel HAZ during heating. The optimized values of the JMA exponent, n, given in Table IV (between 1.11 and 1.14) are lower than those indicated by Christian.[26] The range of n values given by Christian[26] were for isothermal phase transformations. However, rapid heating during welding would cause the transformation to occur with some degree of superheat, which is consistent with lower values of n.

Indeed, when nonisothermal phase transformations were considered, Criado and Ortega[27] indicated the value of n to be 1.0 for instantaneous nucleation and two-dimensional (2-D) diffusion-controlled growth and 1.5 for instantaneous nucleation and 3-D growth. The lower than expected value of n obtained from GA is consistent with the restricted growth of a new phase at the surface constrained by the lack of contiguous material above the top surface where the measurements were made. The optimized values of Q obtained from GA ranged between 99 and 102 kJ/mol. These values were fairly close to the 117 kJ/mole suggested by Nath *et al.*[2] and used by Elmer *et al.*[1] Similarly, the value of ln (k_0) between 11.05 and 11.30 is also in fair agreement with the values of 9.26 and 12.20 suggested by Nath *et al.*[2] and Elmer *et al.*,[1] respectively. Thus, the values of the three JMA parameters calculated in the present study are within the acceptable limits of values reported in the literature.

In most calculations, the starting values of the JMA parameters were chosen to be close to their respective values reported in the literature[2] to achieve rapid convergence. However, in order to explore the dependence of the JMA parameters on the choice of the initial values, in some runs, the initial values of the variables were deliberately defined much further away from their reported values in the literature. The optimized values of the JMA parameters using these starting values of the JMA parameters are given in Table IV. It can be seen that all the sets of optimized JMA parameter values listed in Table IV are internally consistent. When the calculations were started with JMA parameter values very different from their final optimized values, the calculations required more iterations to converge due to the exploration of an expanded search space. However, the JMA parameters obtained from GA were not affected by the choice of their starting values.

C. *Validation of the Optimized JMA Parameters*

The JMA parameters computed from kinetic data at x equal −5.0 and 0.0 mm were used to predict the γ-phase fraction at other monitoring locations, *i.e.,* x equal to −3.5-, −3.0-, −2.5-, and 2.0-mm locations where experimental data were also available. As expected, the calculated austenite fraction curves for the two widely spaced locations, *i.e.,* x equal to −5.0 and 0.0 mm, almost overlap the experimental data in Figure 4. At all other locations, the computed austenite phase fractions agreed well with the corresponding experimental results showing the appropriateness of the values of the JMA parameters determined by GA.

Austenite phase fractions were calculated for all x locations using all sets of JMA parameters listed in Table IV. An average error was calculated by using the calculated and experimentally obtained austenite phase fractions as follows:

$$\text{Average error} = \frac{\sum_{k=1}^{p}\sum_{l=1}^{q}\left|fr^{c}(x_k, y_l, 0) - fr^{e}(x_k, y_l, 0)\right|}{p \times q} \quad [9]$$

where all the variables used in Eq. [9] are defined after Eq. [6]. It was found that the first set, *i.e.,* Q equal to 99.64 kJ/mol, n equal to 1.12, and ln (k_0) equal to 11.07, gave better agreement than the other sets of values. This set was used for calculating the results reported in Figure 4. For the results presented in this figure, the average error between the experimental and the computed austenite phase fractions was 0.06. This error compares favorably with the corresponding average error of 0.10 that resulted from the use of the JMA parameters suggested by Elmer *et al.*[1] The improved values of all three JMA parameters obtained by GA indicates that a more comprehensive three-parameter optimization is more appropriate than the previous two- parameter estimation.

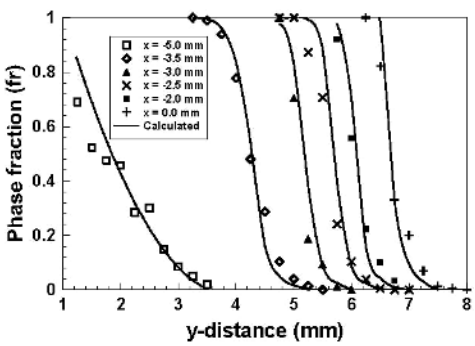

Fig. 4—Comparison of the calculated and experimentally obtained transformed fractions of γ-austenite at six x locations in the weld HAZ. The unknown parameters of the JMA equation were calculated by using the experimental data for only two x locations, *i.e.*, x equal to −5.0 and 0.0 mm. The calculated JMA parameters were then used in the JMA equation to calculate the austenite phase fractions for the other six locations.

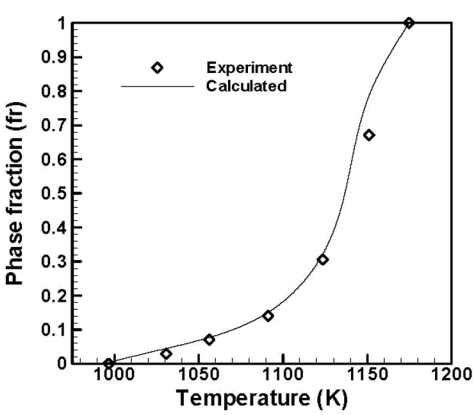

Fig. 5—Comparison of the calculated and experimentally obtained transformed fractions of γ-austenite for constant heating rate of 10 K/s in 1005 steel.

The quality of the JMA parameters obtained by GA depends on the volume and accuracy of high-temperature kinetic data, which are obtained from difficult and specialized experiments. The best possible value of the JMA parameters can be achieved when all the available kinetic data are used to determine these parameters. When the three JMA parameters were determined using all the available experimental data sets, the parameter values were found to be as follows: Q equal to 99.91 kJ/mol, n equal to 1.12, and ln (k_0) equal to 11.06. These parameters gave an average error of 0.05 between the experimental and the predicted values. Since this average error is smaller than that obtained by any other set of JMA parameters obtained to date, these values are recommended for phase fraction calculations during transformation of α-ferrite to γ-austenite during heating of 1005 steel.

To further validate the optimized values of JMA parameters, the γ-austenite phase fractions were calculated for constant heating rate of 10 K/s and compared to experimentally measured data[28] made at the same rate. The experimental data were acquired using an *in-situ* synchrotron based X-ray diffraction method,[28] similar to the technique used to gather the in-situ welding data.[1] These experiments directly measured the fraction of austenite as a function of temperature at a constant heating rate of 10 K/s, while the temperature was recorded using thermocouples attached to the steel sample. Figure 5 shows a good agreement between the calculated and experimental results, which further supports the accuracy of the JMA parameters determined by the GA. Furthermore, this good agreement suggests that the JMA parameters determined in this study can be used to predict phase transformation rates in 1005 steel for both heat treating conditions at rates on the order of 10 K/s and for welding conditions at much higher heating rates.

IV. CONCLUSIONS

A GA based model was used to estimate the parameters of the nonisothermal JMA equation, *i.e.*, the activation energy (Q), pre-exponential term (k_0), and exponent (n), for the transformation of α-ferrite to γ-austenite during heating from a limited volume of experimental kinetic data. The estimated values of JMA parameters lie in the respective range of values reported in the literature. The austenite phase fractions calculated by using the recommended JMA parameters, *i.e.,* Q equal to 99.91 kJ/mol, n equal to 1.12, and ln (k_0) equal to 11.06, show better fit with the experimental data than the JMA parameters reported previously on the basis of a simple graphical technique for estimating the values of n and k_0 assuming a fixed value of Q. Determination of all three JMA parameters by GA provides better results than those previously achieved by the graphical calculation of two of the three JMA parameters.

ACKNOWLEDGMENTS

The authors express their gratitude to Mr. W. Zhang for assisting with the phase transformation calculation model. The authors are also thankful to Dr. K. Deb for providing free access to their PCX operator module. This research was supported by a grant from the United States Department of Energy, Office of Basic Energy Sciences, Division of Materials Sciences, under Grant No. DE-FGO2–01ER45900.

APPENDIX A

Algorithm of the G3 Model

The GA used in the present study is a PCX operator based G3 model.[22] The steps involved are as follows.

(1) The best parent and $\mu - 1$ other randomly selected parents are chosen from the population. A population is a collection of many individuals and each individual represents a set of randomly chosen values of the three nondimensionalized JMA parameters. A parent refers to an individual in the current population. The best parent is the individual that has the best fitness, *i.e.*, gives the minimum value of the objective function, in the entire population.
(2) From the chosen μ parents, λ offsprings (new individuals) are generated using a recombination scheme. In the present study, a parametric study on the G3 model showed that for $\mu = 3$ and $\lambda = 2$, the model required minimum number of iterations to converge. Therefore, $\mu = 3$ and $\lambda = 2$ were used in the present study. A recombination scheme is a process for creating new individuals from the parents.
(3) Two parents are randomly chosen from the current population.
(4) A combined subpopulation having λ offsprings (step 2) and the two randomly chosen parents (step 3) is formed.
(5) The best two solutions, *i.e.*, the solutions having least values of the objective function, are chosen from the subpopulation (step 4) and these replace the randomly chosen two parents (step 3) of the current population. This gives the new population for the next iteration or generation.

The preceding steps, as applied to the present problem, are shown in Figure 6. The figure clearly illustrates the working of the model to optimize the three unknown JMA parameters. The recombination scheme (step 2) used in the present model is based on PCX operator.[22] A brief description of this operator, tailored to the present problem, is as follows:

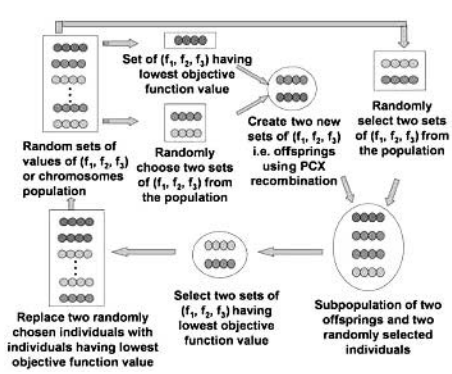

Fig. 6—G3 model using PCX operator.

The first three parents, *i.e.*, (f_1^0, f_2^0, f_3^0), (f_1^1, f_2^1, f_3^1), (f_1^2, f_2^2, f_3^2) are randomly selected from the current population. Here, the subscripts represent the three variables defined in Eq. [7], while the superscripts denote the parent identification number. The scheme for the creation of the new individual (offspring), *i.e.*, $\mathbf{y} = (f_1', f_2', f_3')$, by using the PCX operator on these three parents, is shown in Figure 7. The mean vector or centroid, $\mathbf{g} = \left(\frac{f_1^0 + f_1^1 + f_1^2}{3}, \frac{f_2^0 + f_2^1 + f_2^2}{3}, \frac{f_3^0 + f_3^1 + f_3^2}{3}\right)$, of the chosen three parents is computed. To create an offspring, one of the parents, say, $\mathbf{x}^{(p)} = (f_1^0, f_2^0, f_3^0)$, is chosen randomly. Then, the direction vector, $\mathbf{d}^{(p)} = \mathbf{x}^{(p)} - \mathbf{g}$, is calculated from the selected parent to the mean vector or centroid. Thereafter, from each of the other two parents, *i.e.*, (f_1^1, f_2^1, f_3^1) and (f_1^2, f_2^2, f_3^2), perpendicular distances, D_i, to the direction vector, $\mathbf{d}^{(p)}$, are computed and their average, $\bar{D}$, is found. Finally, the offspring is created as follows:[22]

$$\mathbf{y} = \mathbf{x}^{(p)} + w_\zeta |\mathbf{d}^{(p)}| + \sum_{i=1, i\neq p}^{3} w_\eta \bar{D}\, \mathbf{h}^{(i)} \qquad [A1]$$

where $\mathbf{h}^{(i)}$ are the two orthonormal bases that span the subspace perpendicular to $\mathbf{d}^{(p)}$, and the parameters w_ζ and w_η are randomly calculated zero-mean normally distributed variables. The obtained value of the offspring, $\mathbf{y} = (f_1', f_2', f_3')$, using the chosen three parents, is as follows:

$$f_1' = f_1^0 + f_{11} + f_{12} \qquad [A2a]$$

$$f_2' = f_2^0 + f_{21} + f_{22} \qquad [A2b]$$

$$f_3' = f_3^0 + f_{31} + f_{32} \qquad [A2c]$$

where

$$f_{11} = w_\zeta \left(\frac{2f_1^0 - f_1^1 - f_1^2}{3}\right) \qquad [A3a]$$

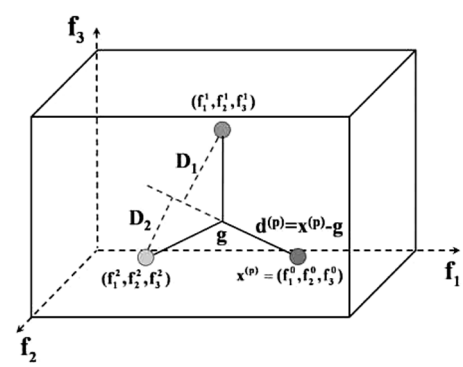

Fig. 7—PCX operator: a generic parent centric approach where new sets of variables values are created near the parents shown by solid circles. The direction vector, $\mathbf{d}^{(p)} = \mathbf{x}^{(p)} - \mathbf{g}$ is calculated from the selected parent, *i.e.*, $x^{(p)} = (f_1^0, f_2^0, f_3^0)$, to centroid, $g = \left(\frac{f_1^0 + f_1^1 + f_1^2}{3}, \frac{f_2^0 + f_2^1 + f_2^2}{3}, \frac{f_3^0 + f_3^1 + f_3^2}{3}\right)$.

$$f_{21} = w_\zeta\left(\frac{2f_2^0 - f_2^1 - f_2^2}{3}\right) \quad [A3b]$$

$$f_{31} = w_\zeta\left(\frac{2f_3^0 - f_3^1 - f_3^2}{3}\right) \quad [A3c]$$

$$f_{12} = w_\eta\left(\frac{a_2 + b_2}{2}\right)\left[1 - \left(\frac{2f_1^0 - f_1^1 - f_1^2}{3d}\right)^2\right] \quad [A3d]$$

$$f_{22} = w_\eta\left(\frac{a_2 + b_2}{2}\right)\left[1 - \left(\frac{2f_2^0 - f_2^1 - f_2^2}{3d}\right)^2\right] \quad [A3e]$$

$$f_{32} = w_\eta\left(\frac{a_2 + b_2}{2}\right)\left[1 - \left(\frac{2f_3^0 - f_3^1 - f_3^2}{3d}\right)^2\right] \quad [A3f]$$

The various unknown variables used in Eqs. [A3a] through [A3f] can be represented in simplified form as follows:

$$d = \sqrt{\left(\frac{2f_1^0 - f_1^1 - f_1^2}{3}\right)^2 + \left(\frac{2f_2^0 - f_2^1 - f_2^2}{3}\right)^2 + \left(\frac{2f_3^0 - f_3^1 - f_3^2}{3}\right)^2} \quad [A4a]$$

$$a_2 = e_1 \times \sqrt{1 - (a_1)^2} \quad [A4b]$$

$$b_2 = e_2 \times \sqrt{1 - (b_1)^2} \quad [A4c]$$

$$a_1 = \frac{\left(f_1^1 - f_1^0\right)\left(\frac{2f_1^0 - f_1^1 - f_1^2}{3}\right) + \left(f_2^1 - f_2^0\right)\left(\frac{2f_2^0 - f_2^1 - f_2^2}{3}\right) + \left(f_3^1 - f_3^0\right)\left(\frac{2f_3^0 - f_3^1 - f_3^2}{3}\right)}{d \times e_1} \quad [A4d]$$

$$e_1 = \sqrt{\left(f_1^1 - f_1^0\right)^2 + \left(f_2^1 - f_2^0\right)^2 + \left(f_3^1 - f_3^0\right)^2} \quad [A4e]$$

$$b_1 = \frac{\left(f_1^2 - f_1^0\right)\left(\frac{2f_1^0 - f_1^1 - f_1^2}{3}\right) + \left(f_2^2 - f_2^0\right)\left(\frac{2f_2^0 - f_2^1 - f_2^2}{3}\right) + \left(f_3^2 - f_3^0\right)\left(\frac{2f_3^0 - f_3^1 - f_3^2}{3}\right)}{d \times e_2} \quad [A4f]$$

$$e_2 = \sqrt{\left(f_1^2 - f_1^0\right)^2 + \left(f_2^2 - f_2^0\right)^2 + \left(f_3^2 - f_3^0\right)^2} \quad [A4g]$$

In the PCX approach, individual recombination operator biases offspring to be created near the parents by assigning each parent an equal probability of creating offspring in its neighborhood.[22] As a consequence, the PCX based G3 model converges faster for standard test functions as compared to other evolutionary algorithms.[22,23]

REFERENCES

1. J.W. Elmer, T.A. Palmer, W. Zhang, B. Wood, and T. DebRoy: *Acta Mater.*, 2003, vol. 51, pp. 3333-49.
2. S.K. Nath, S. Ray, and V.N.S. Mathur: *Iron Steel Inst. Jpn.*, 1994, vol. 34, pp. 191-97.
3. A. De and T. DebRoy: *J. Phys. D: Appl. Phys.*, 2004, vol. 37, pp. 140-50.
4. A. Kumar, W. Zhang, C.-H. Kim, and T. DebRoy: *7th Int. Sem. on Numerical Analysis of Weldability*, Graz, Austria, Sept. 29–Oct. 1, 2003, H. Cerjak, H.K.D.H. Bhadesia, and E. Kozeschnik, eds., Technical University of Graz Press, Graz, Austria, 2004, pp. 1-24.
5. A. Kumar and T. DebRoy: *Int. J. Heat Mass Transfer*, 2004, vol. 47, pp. 5793-806.
6. D.E. Goldberg: *GA in Search, Optimization and Machine Learning*, Addison-Wesley, Boston, MA, 1989.
7. *Handbook of Evolutionary Computation*s, T. Back, D.B. Fogel, and Z. Michalewicz, eds., IOP Publishing Ltd., Oxford University Press, Oxford, United Kingdom, 2000.
8. W. Zhang, J.W. Elmer, and T. DebRoy: *Mater. Sci. Eng. A*, 2002, vol. 333, pp. 321-35.
9. Z. Yang, J.W. Elmer, J. Wong, and T. DebRoy: *Welding J.*, 2000, vol. 79, pp. 97s-112s.
10. A. De and T. DebRoy: *J. Appl. Phys.*, 2004, vol. 95, pp. 5230-40.
11. S. Mishra and T. DebRoy: *Acta Mater.*, 2004, vol. 52, pp. 1183-92.
12. Z. Yang, S. Sista, J.W. Elmer, and T. DebRoy: *Acta Mater.*, 2000, vol. 48, pp. 4813-25.
13. X. He, P.W. Fuerschbach, and T. DebRoy: *J. Appl. Phys.*, 2003, vol. 94, pp. 6949-58.
14. A. Kumar and T. DebRoy: *J. Appl. Phys.*, 2003, vol. 94, pp. 1267-77.
15. S.A. David, R. Trivedi, M.E. Eshelman, J.M. Vitek, S.S. Babu, T. Hong, and T. DebRoy: *J. Appl. Phys.*, 2003, vol. 93, pp. 4885-95.
16. W. Zhang, G.G. Roy, J.W. Elmer, and T. DebRoy: *J. Appl. Phys.*, 2003, vol. 93, pp. 3022-33.
17. X. He, P.W. Fuerschbach, and T. DebRoy: *J. Phys. D: Appl. Phys.*, 2003, vol. 36, pp. 1388-98.
18. T. Hong and T. DebRoy: *Metall. Mater. Trans. B*, 2003, vol. 34B, pp. 267-69.
19. W. Pitscheneder, T. DebRoy, K. Mundra, and R. Ebner: *Welding J.*, 1996, vol. 75, pp. 71s-80s.
20. K. Mundra, T. DebRoy, and K.M. Kelkar: *Num. Heat Transfer A*, 1996, vol. 29, pp. 115-29.
21. W. Zhang, J.W. Elmer, and T. DebRoy: *Scripta Mater.*, 2002, vol. 46, pp. 753-57.
22. K. Deb, A. Anand, and D. Joshi: *KanGAL Report No. 2002003*, Indian Institute of Technology, Kanpur, India, 2002.
23. K. Deb: *KanGAL Report No. 2003003*, Indian Institute of Technology, Kanpur, India, 2003.
24. S.V. Patankar: *Numerical Heat Transfer and Fluid Flow*, Hemisphere, New York, NY, 1980.
25. J.W. Elmer, J. Wong, and T. Ressler: *Metall. Mater. Trans. A*, 2001, vol. 32A, pp. 1175-88.
26. J.W. Christian: *The Theory of Transformations in Metals and Alloys*, 3rd ed., Pergamon, Boston, MA, 2002.
27. J.M. Criado and A. Ortega: *Acta Metall.*, 1987, vol. 35, pp. 1715-21.
28. Unpublished data from J.W. Elmer, T.A. Palmer, S.S. Babu, and E.D. Specht: Lawrence Livermore National Laboratory, Livermore, CA, Feb. 2004.